



City Research Online

City, University of London Institutional Repository

Citation: Weng, Y., Fu, F. & Qian, K. (2023). Punching Shear Resistance of Corroded Slab-Column Connections Subjected to Eccentric Load. *Journal of Structural Engineering*, 149(1), 04022219. doi: 10.1061/(asce)st.1943-541x.0003504

This is the accepted version of the paper.

This version of the publication may differ from the final published version.

Permanent repository link: <https://openaccess.city.ac.uk/id/eprint/28409/>

Link to published version: [https://doi.org/10.1061/\(asce\)st.1943-541x.0003504](https://doi.org/10.1061/(asce)st.1943-541x.0003504)

Copyright: City Research Online aims to make research outputs of City, University of London available to a wider audience. Copyright and Moral Rights remain with the author(s) and/or copyright holders. URLs from City Research Online may be freely distributed and linked to.

Reuse: Copies of full items can be used for personal research or study, educational, or not-for-profit purposes without prior permission or charge. Provided that the authors, title and full bibliographic details are credited, a hyperlink and/or URL is given for the original metadata page and the content is not changed in any way.

Punching Shear Resistance of Corroded Slab-Column Connections Subjected to Eccentric Load

Yun-Hao Weng¹, Feng Fu², C. Eng., F. ASCE, Kai Qian^{3*}, M. ASCE

ABSTRACT

Due to deicing salt, marine and offshore environment may cause rebar corrosion in reinforced concrete (RC) flat-slab floor system. Therefore, it increases the possibility of punching shear failure of slab-column connections. However, little research results are available for RC slab-column connections with corroded rebars under eccentric load, which is very common in realistic loading conditions. To fill the gap, 15 full-scaled RC flat slab-column connections were fabricated and tested to investigate the performance of corroded slab-column connections under eccentric load. The design variables include reinforcement ratio, loading eccentricity, and degree of rebar corrosion. There are two stages for the experimental process including: 1) accelerated rebar corrosion test; and 2) quasi-static test. It is found from the test results that, in general, rebar corrosion has detrimental effects on the punching shear strength and stiffness of the connections. In addition, corrosion of reinforcement may change the failure mode of the slab-column connection. However, it is unexpected that the energy-dissipating capacity and deformation capacity of the slab-column connection with high reinforcement ratio and small loading eccentricity increased with increasing the corroded degree.

Author Keywords: Punching shear resistance; Reinforced concrete slab-column connection; Accelerated corrosion test; Eccentric load; Experimental results.

¹PhD student, College of Civil Engineering and Architecture at Guangxi University, Nanning, China 530004, Email: wengyh@st.gxu.edu.cn

²Senior Lecturer (Associate Professor) in Structural Engineering, School of Mathematics, Computer Science and Engineering, City, University of London, U.K., Feng.Fu.1@city.ac.uk

³Professor, College of Civil Engineering and Architecture at Guilin University of Technology, China, 541004; previous Professor, Guangxi University, Nanning, China 530004, Email: qiankai@glut.edu.cn

INTRODUCTION

The reinforced concrete (RC) flat-slab floor system offers an economical and reliable structural option. Since 20th century, it is widely used in apartments, parking lots, bridges, dormitories, and other places with the advantages of simple formwork, flexible layout, floor height reduction, and shortened construction time. However, as no down stand beams are designed it brings a structural problem that higher shear and flexural stresses are concentrated in the slab-column connections. This can lead to brittle punching failure, leading to catastrophic consequences (Qian and Li 2015; Liu *et al.* 2015; Xue *et al.* 2018, 2020). The shear and flexural stresses in the slab-column connections were inevitably caused by the combined action of shear force and unbalanced moment due to the horizontal load or unsymmetric factors of the structure. The combined action of unbalanced bending moment and axial force was normally represented by eccentric load. Meanwhile, the flat-slab floor systems might be under harsh environmental conditions, such as de-icing salts, coastal environmental, freeze thaw cycles, and wet-dry cycles, etc., which may cause rebar corrosion. The rebar corrosion is prone to many adverse consequences, such as reducing effective area, yield strength, and ductility of steel bars (Cairns *et al.* 2005), which in turn is detrimental to punching shear strength of the connection or flexural strength of the slab.

Many efforts have been devoted to understanding the punching shear resistance of slab-column connections under either concentric or eccentric load (Jang and Shen 1986; Bazant and Cao 1987; Durrani *et al.* 1995; Marzouk *et al.* 1998, 2000; Hawkins *et al.* 1989; Tian *et al.* 2008; Teng *et al.* 2018; Drakatos *et al.* 2018). However, there are few quantitative studies on the impact of reinforcement corrosion on the shear resistance of slab-column connections, as most of the available researches have focused on RC slabs, columns, and beams (Okada *et al.* 1988;

Almusallam *et al.* 1996; Castel *et al.* 2000a, 2000b; Lee *et al.* 2000; Marano *et al.* 2008; Ikehata *et al.* 2020).

Since the realistic rebar corrosion procedure in RC structures is usually very slow, the artificial electrified accelerated corrosion method is commonly used to accelerate the corrosion procedure and produce equivalent corroded RC components in the laboratory (Maaddawy and Soudki 2003; González *et al.* 1995; Al-Swaidani and Aliyan 2015; Ou *et al.* 2016). In this method, the electrochemical potential is used to the rebar and external cathode, and the corrosion rate is controlled by the applied constant current density. The corroded mass loss of rebar was commonly determined based on Faraday's equation (Maaddawy and Soudki 2003):

$$t = \frac{zFm}{MI} \quad (1)$$

where t is corroded time (s); z is the ionic charge; F is the constant of Faraday; m is weight of rusty steel (g); M is the atomic weight of steel; and I is the amperes of current (A).

So far, little research has been carried out on RC slab-column connections with corroded rebars under punching shear forces and unbalanced moments, which could be expressed by eccentric load. Therefore, to partially fulfill the gap, a series of RC slab-column connections with different corroded degree and unbalanced moments (or eccentricity), were fabricated and tested in the present study.

EXPERIMENTAL PROGRAM

Specimen design and material properties

A total of 15 RC full scaled slab-column connections are fabricated and tested. The size and detailed drawing of typical specimens are shown in Fig. 1. The key characteristics of the specimens are tabulated in Table 1. These specimens were categorized into five series according to loading eccentricity and reinforcement ratio: C-0.91, C-0.52, E1-0.91, E2-0.91, and E2-0.52. In each series,

three different corroded degrees were designed, including 0% (control specimen), 10%, and 20%. Therefore, the label of each specimen consists of three parts: The first part represents loading eccentricity: “C” for concentric loading; and “E1” and “E2” for loading eccentricity of 100 mm and 200 mm, respectively. The second one is a number to denote the flexural reinforcement ratio of the slabs: 0.52% and 0.91%. The last one is a number to denote the corroded degree (0, 10%, and 20%). For example, E1-0.91-10 represents a specimen with a reinforcement ratio of 0.91%, a designated corroded degree of 10%, and a loading eccentricity of 100 mm. As shown in Fig. 1, the size of the slab is 150×2200×2200 mm while the dimension of the center column is 200 mm. The column stub extended 150 mm and 300 mm from the top surfaces for the specimens subjected to concentric load and eccentric load, respectively. And a corbel was cast beside the column stub to apply eccentric load. The corbel and column stub were reinforced by 8T20, and the transverse reinforcement was R8@50 mm. Two layers of reinforcement mesh were used to reinforce the slab. For the top layer reinforcement, T10@260 mm mesh is designed. For the bottom layer, T12@105 mm mesh is designed for specimens with reinforcement ratio of 0.91%. For the specimens with the reinforcement ratio of 0.52%, T12@190 mm mesh is utilized. “T10”, “T12”, and “T20” represent deformed rebar with a diameter of 10 mm, 12 mm, and 20 mm, respectively, while “R8” represents plain rebar with a diameter of 8 mm.

Based on cylinder tests, the average compressive strengths on the testing day of the specimens are shown in Table 1. The yield strength of T10 and T12 is 558 MPa and 532 MPa, respectively, whereas the ultimate strength of the T10 and T12 is 717 MPa and 695 MPa, respectively. In addition, the ultimate elongation is 15.0% for T10 and 22.1% for T12 before corrosion.

Test apparatus for accelerated corrosion

The steel bar is corroded by electrified accelerated corrosion method. Based on Teng *et al.*

(2018), only the rebar within $1.5d_o$ (where d_o is slab thickness) distance from the column edge can effectively resist the punching shear. Thus, to improve the efficiency and reduce the cost, the corroding area was restricted to $c + 4d_o$ (800 mm, where c is the column size) in each direction, which is larger than the critical region. As shown in Fig. 2, an 800 mm square tank with 5% sodium chloride solution was placed on the upturned specimen. A wet sponge was used to cover the tank to decrease water evaporation. A stainless-steel gauze was dipped into the solution and connected to the cathode of a direct current (DC) power supply, while the reinforcements in the corroded area were connected to the anode of the DC power supply. The applied constant current density was set as 0.6 mA/cm^2 . The predicted required corroding time for specimens with the corroded degree of 10% and 20% were 17 and 34 days, respectively, according to Eq. (1).

Test setup and instrumentations

The punching shear resistances of the specimens were evaluated by a quasi-static loading method. Fig. 3 shows the typical test setup for the specimens in the E series (eccentric loading case). As it can be seen in the figure, the specimen was placed on eight height-adjustable simple supports. The concentrated load is applied on the column stub or corbel using a hydraulic jack. A steel assembly was particularly designed to guarantee that the load applied was vertical. In addition, different from the specimens in the C series (concentric loading case), an additional one-way hinge was designed for the specimens in the E series to allow rotation of the column during testing.

A series of Linear Variable Differential Transformers (LVDTs) are installed in target positions to monitor the deflection of the specimens. For uncorroded specimens, the strain of slab reinforcements was measured during tests. However, the strain of corroded specimens was not monitored as the accelerated corrosion procedure may damage the strain gauge. A load cell, which was installed beneath the hydraulic jack, was utilized to measure applied load. A data logger with

60 channels and a sampling frequency of 5 Hz was utilized to record the data of all instrumentations. In addition, a crack detector was utilized to measure the crack width until failure.

TEST RESULTS AND DISCUSSION

Corrosion result

In the accelerated corrosion process, a large amount of corrosion product appeared at the corrosion zone. As illustrated in Fig. 4, a number of thin cracks parallel to the rebars were observed on the slab surface after cleaning away the corrosion product. Comparing the specimens with different corroded degrees, it could be found that the width of cracks increased with increasing corroded degree. The widths of the initial cracks due to rebar corrosion ranged from 0.04 mm to 0.13 mm.

The corroded rebars within the corrosion zone (800 mm square in the center) were removed after loading test to measure the actual corroded degree. The extracted bars were cut into segments with 100 mm long. Based on the distance from the column center, the segments were grouped carefully. Afterward, the rebar segments were then immersed in a 10% hydrochloric acid solution for 24 hours to remove the corrosion product and then rinsed thoroughly. The rebar segments were then put into a thermostatic container with 60 °C for 24 hours to dry it fully before weighing. The actual corroded degree can be defined according to Eq. (2):

$$w = \frac{W_0 - W}{W_0} \times 100 \quad (2)$$

where w is corroded degree (%); W_0 is weight of the reinforcement segment in original; and W is weight of corroded rebar segment.

Table 2 summarizes the measured corrosion of the specimens. As can be seen, the maximum corroded degree occurred in the rebar around the column edge. Moreover, the maximum corroded degree could exceed the designated corroded degree. However, the average corroded degrees are

always less than the specified values. This may be due to the diffusion of NaCl solution from the tank to the outside of the tank, resulting in a loss of current.

Crack pattern and failure mode

Figs. 5 and 6 show the crack pattern of the specimens in the C and E series, respectively, at failure. The downward arrows in Fig. 6 represent the directions of unbalanced moments (right-hand principle). Moreover, the relationship between crack width and load before failure is shown in Fig.7. In general, for the uncorroded specimens, the first batch of cracks was occurred at the bottom side of the slab-column interfaces at about 40% of the failure load. For the corroded specimens, the initial cracks caused by the rebar corrosion developed wider at about 30% of the failure load. Further increasing the applied load, the cracks were developed towards the slab edge. Finally, circumferential cracks developed from internal oblique shear cracks were observed when specimens reaching their punching shear strength. Different from the specimens in the C series, Fig. 6 shows more damage occurring in the specimens at the side of the eccentric load (right side of each photo) due to the extra flexural tensile stresses from the moment transfer. Comparing between E1 and E2 series, the specimens in the E2 series showed more serious asymmetrical damage. As shown in Fig. 7, wider cracks are measured in the specimens with higher corroded degrees under the same load level because of the deterioration of the cracked stiffness caused by rebar corrosion. Furthermore, specimens with higher loading eccentricity have wider cracks under the same load level due to greater extra tensile stresses transferred from the unbalanced moment.

As illustrated in Figs. 5 and 6, all connections exhibited punching shear failure with wide circumferential cracks. R_{cone} is called critical failure zone, which is characterized by its radius from the slab-column interface to the circumferential crack. The R_{cone} is measured at different positions, and thus, only the average value was determined and tabulated in Table 3. As can be seen, the R_{cone}

of uncorroded specimens are smaller than those of corroded specimens. This could be explained as the presence of the horizontal crack along the reinforcements due to expansive force after corrosion. When the internal oblique shear cracks intersect with the initial horizontal crack, the shear crack may along the horizontal crack before continuing to extend in depth, enlarging the critical failure zone. Similar findings were concluded in Ikehata *et al.* (2020).

Punching shear strength

Table 3 tabulated the measured punching shear strengths of tested specimens. For easier comparison of the specimens cast in different batches, the punching shear strength was normalized as below: $v_c/\sqrt{f'_c}$. As can be seen in Table 3, comparing to C-0.91-0, the normalized punching shear strengths of E1-0.91-0 and E2-0.91-0 decreased by 16% and 32%, respectively. For specimens with a reinforcement ratio of 0.52%, the normalized punching shear strength of E2-0.52-0 is 80% of C-0.52-0. Therefore, the existence of an unbalanced moment would decrease the punching shear strengths of the slab-column connections significantly.

As shown in Table 3, increasing the corroded degree, the normalized punching shear strength decreased. For C-0.91 series, the normalized punching shear strength respectively decreased by 14% and 25%, when the average corroded degree was 9.6% and 17.6%. For C-0.52 series, the normalized punching shear strength decreased by 26% when the corroded degree increased from 0% to 13.0%. For the eccentric loading series of E1-0.91, increasing the corroded degree from 0% to 16.4%, the normalized punching shear strength decreased by 22%. Similarly, for E2-0.91 series, when the corroded degree increased from 0% to 17.9%, the normalized punching shear strength decreased by 23%. For E2-0.52 series, when the corroded degree increased to 15.4%, the normalized punching shear strength decreased by 24%. Thus, the rebar corrosion may jeopardize the normalized punching shear strength significantly. The reduction of punching shear strength

comes from the decrease of the shear resistance of concrete and reinforcement. The cracks due to rebar corrosion may be adverse to the shear resistance of concrete slabs by weakening aggregate interlocking. In addition, due to the reduced cross-section of the corroded steel bars, less dowel action could be developed. The bond loss between concrete and corroded steel bars further weakened the shear resistance of the rebar. As the real rebar corrosion is different with the purpose designed corrosion for tested specimens, based on linear regression, the decreasing of normalized punching shear strength per 1% corrosion was determined for each corroded specimen. The decreasing of normalized punching shear strength per 1% corrosion was 1.42%, 1.90%, 1.3%, 1.27%, and 1.56% for C-0.91, C-0.52, E1-0.91, E2-0.91 and E2-0.52 series, respectively. This indicated that the rebar corrosion has more influence on the punching shear strength of the connections with lower reinforcement ratio and less loading eccentricity.

Strain gauge results

Fig. 8 shows the variation of strain of the rebar in uncorroded specimens at failure. As the results of the malfunctioned strain gauges were removed, some of the curve is not continual. As can be seen, different from the concentric loading cases, the strain results of the specimens subjected to eccentric load were unsymmetrical. The reinforcement strains at the side of the eccentric load were larger than those of another side, as the unbalanced moment increased the deflection in the reinforcements. In addition, the specimens with larger loading eccentricity achieved larger strain at the side of the eccentric. For C-0.91, E1-0.91, and E2-0.91 series, the yield strength is only measured at the rebar nearby the column face. This confirmed that the controlled failure mode is punching shear failure. However, for C-0.52 and E2-0.52 series, the yield strength was reached in the rebar extensively. Therefore, the failure modes of these specimens were called flexural-punching failure, which is defined as occurring punching shear

failure after the flexural reinforcement extensively yielded.

Load-displacement relationship

Fig. 9 comparison of the load-displacement relationships of the specimens. It should be noted that the displacement results were measured by the LVDT installed at the column center. Specimens with higher corroded degrees obtained lower initial stiffness since wider cracks occurred in the corrosion process. Moreover, it was found that increasing the corroded degrees, the post-cracking stiffness decreases significantly as the reduction of the cross-sectional area and elastic modulus of rebar caused by rebar corrosion.

The deformation capacity, which is defined as the displacement in accordance with the failure load, varied with the increase of the corroded degree. For C-0.91 and E1-0.91 series, increasing the corroded degree causes an increase in the deformation capacity. It resulted in greater ductility of the specimens, which could be explained as the effective reinforcement ratio decreased after rebar corrosion. On the contrary, the higher corroded degree results in a smaller deformation capacity for E2-0.91 series due to its larger unbalanced moment. For the specimens with a low reinforcement ratio, the deformation capacity decreased with increasing the corroded degree. This is because these specimens had attained the flexural strength before the punching shear strength while the yield strength of reinforcement deteriorated after rebar corrosion.

Table 3 tabulated the energy absorbed capacity, which is defined as the area enclosed by the load-displacement curve. It can be seen from the table, for C-0.91 series, the energy-dissipating capacity increases with the increase of corroded degree due to greater deformation capacity after corrosion. However, for C-0.52 series, the energy absorbed capacity kept decreasing with increasing the degree of rebar corrosion, as both the load resistance and deformation capacity decreased. Moreover, the E1-0.91 series showed a similar phenomenon to the C-0.91 series, while

the E2-0.91 and E2-0.52 series are similar to the C-0.52 series.

Deflection shapes

Fig. 10 compares the deflection shapes at the centerlines of different specimens in the direction of loading eccentricity at failure load. For eccentric loading cases, different from the symmetrical deflection of the specimens in the C series, the deflection in the side of the eccentric load is larger than those of other sides as a result of the unbalanced moment. The rotation angle of the column is 0.7° , 0.78° , 0.86° , 1.0° , 1.07° , 1.14° , 1.23° , 1.35° , and 1.54° for E1-0.91-0, E1-0.91-10, E1-0.91-20, E2-0.91-0, E2-0.91-10, E2-0.91-20, E2-0.52-0, E2-0.52-10, and E2-0.52-20, respectively. Thus, the specimens with higher corroded degrees reach a greater relative rotation at failure load. It might be attributed to the reduction of the rotational stiffness of the column-slab connection caused by the rebar corrosion.

ANALYTICAL ANALYSIS AND DISCUSSION

Yield-line analysis

The yield-line method is utilized here for prediction of the flexural strength of the specimens. According to Park and Gamble (1981), the typical yield-line patterns for specimens are shown in Fig. 11. The yield lines outside the circular line are ignored. As given in Fig. 11(a), the corroded specimens in C series consisted of corroded and uncorroded areas. Based on the virtual work principle, the flexural strength P_{flex} can be calculated as follows:

$$P_{flex} = \left[4m_u c + 2\pi m_{u,c} r_c + 2\pi m_u (r - r_c) \right] / r \quad (3)$$

where c is the column size; r_c is the equivalent radius of the corroded area, that is determined by $r_c = 2(l-c)/\pi = 382$ mm herein (l is the size of the corroded area); r is the radius of the positive moment region (870 mm herein); m_u and $m_{u,c}$ are the nominal flexure capacity of the slab for uncorroded and corroded section, respectively. In accordance with CSA (2014), m_u and $m_{u,c}$ can

be determined as follows:

$$m_u = \rho f_y d^2 (1 - \alpha_1 \rho f_y / f_c') \quad (4)$$

$$m_{u,c} = \rho_c f_{y,c} d^2 (1 - \alpha_1 \rho_c f_{y,c} / f_c') \quad (5)$$

$$\alpha_1 = 0.85 - 0.0015 f_c' \quad (6)$$

where ρ_c and ρ are the reinforcement ratio of corroded and uncorroded section, respectively; $f_{y,c}$ and f_y are the yield strength for the corroded and uncorroded reinforcement; d is the effective depth of the slab; and f_c' is the compressive strength of concrete.

For the corroded section, the yield strength of the reinforcement $f_{y,c}$ and the effective reinforcement ratio ρ_c could be determined by Eq. (7) and (8), respectively.

$$f_{y,c} = f_y (1 - \alpha_y (w/100)) \quad (7)$$

$$\rho_c = \rho (1 - w/100) \quad (8)$$

where w is the corroded degree; α_y is an empirical coefficient, according to Lee *et al.* (1998), it is 1.24 for uniform corrosion and 1.98 for pitting corrosion.

According to Park and Gamble (1981), for E series, the radius of the positive moment area is satisfied by $r = \sqrt{1.5c} \approx 250 \text{ mm}$, which is smaller than the corroded area in this study. Therefore, the maximum flexural moment M_{flex} of all specimens in the E series could be calculated by the formula proposed by Park and Gamble (1981), as shown in follows:

$$M_{flex} = \begin{cases} 9.04m_u c - 0.5V_u c & \text{for uncorroded specimens} \\ 9.04m_{u,c} c - 0.5V_u c & \text{for corroded specimens} \end{cases} \quad (9)$$

where V_u is the applied shear force.

The predicted values of the tested specimens based on the yield-line analysis are summarized in Table 3. The ratio of predicted value to tested value (V_u/P_{flex} or M_u/M_{flex}) is used as an index to determine the failure modes. If the ratio is greater than or equal to 1, the failure is flexural-punching, otherwise, the failure is controlled by punching shear. As can be seen in Table 3, the

ratios of C-0.91-0, C-0.52-0, E1-0.91-0, E2-0.91-0, and E2-0.52-0 are 0.86, 1.06, 0.50, 0.75, and 1.22, respectively. Therefore, the failure mode of C-0.52-0 and E2-0.52-0 is flexural-punching failure, while that of C-0.91-0, E1-0.91-0, and E2-0.91-0 is punching shear failure, which is consistent with the results based on strain gauge results. For corroded specimens, the ratios of C-0.52-10, E2-0.91-20, E2-0.52-10, and E2-0.52-20 are greater than or equal to 1, indicating their predominant flexural-punching failure, while those failed in punching shear do have ratios less than 1. Moreover, increasing the corroded degree, the ratios of the specimens in C series decreased, while those of the specimens in E series increased.

Design formula in important codes

In this section, the reliability of formulae proposed by ACI 318-19 (2019), GB 50010 (2010), Eurocode 2 (2004), BS 8110 (1997), and Model Code 2010 (2012) for prediction of the punching shear strength of uncorroded or corroded slab-column connections are evaluated.

ACI 318-19 (2019)

For American Code, ACI 318-19 (2019), the critical section was determined by straight lines drawn parallel to and at a distance $d/2$ from the edges of the columns. For column-slab connection under gravity load only, the punching shear stress v_c can be calculated by Eq. (10).

$$v_c = \min \left\{ 0.17 \left(1 + \frac{2}{\beta} \right) \lambda_s, 0.083 \left(2 + \frac{\alpha_s d}{b_0} \right), 0.33 \lambda_s \right\} \lambda \sqrt{f'_c} \quad (10)$$

where β is a ratio of long side to short side of the column; λ_s is a factor considering size effect, $\lambda_s = \sqrt{2/(1+0.004 \cdot d)} \leq 1.0$; λ is the density factor of concrete (for normal concrete and semi-lightweight concrete, it is 1.0 and 0.85, respectively); α_s is constant used for column location (for interior, edge, and corner columns, it is 40, 30, and 20, respectively); b_0 is the control perimeter; d is the effective depth of the slab; and f'_c is the concrete compressive strength.

For the interior connection with square column under eccentric load, the v_u is estimated by

Eq. (11).

$$v_u = v_{uv} + \frac{\gamma_v M_{sc} (c + d) / 2}{J_c} \quad (11)$$

where v_{uv} is the shear stress on the slab critical section; M_{sc} is the moment resisted by the column; γ_v factor used to quantify the unbalanced moment transferred by the eccentricity of shear at slab-column connections (0.4 for square column); J_c is property of assumed critical section analogous to the polar moment of inertia; and c is the size of the square column.

GB 50010 (2010)

Similar to American Code, the assumed critical section of Chinese Code, GB 50010 (2010), is also defined as at a distance $d/2$ from the column edge. For concentric loading cases, the punching shear strength V_l of the specimens excluded shear reinforcement can be calculated as follows:

$$V_l \leq 0.7 \beta_h f_t \eta u_m d \quad (12)$$

$$\eta = \min \left\{ 0.4 + \frac{1.2}{\beta_s}, 0.5 + \frac{\alpha_s d}{4u_m} \right\} \quad (13)$$

where β_h is the influence coefficient of slab thickness, 1.0 for slab thickness $d_0 \leq 800$ mm and 0.9 for $d_0 \geq 2000$ mm; f_t is the axial tensile strength of concrete; u_m is the critical shear perimeter; d is the effective depth; β_s is the ratio of long to short sides of the column; and α_s is an adjustment factor (40, 30, and 20 for interior, edge, and corner columns, respectively).

For interior connections subjected to eccentric load, the equivalent punching shear strength $V_{l,eq}$ could be determined by Eq. (14).

$$V_{l,eq} = V_l + \frac{\alpha_0 M_{unb} (c + d) / 2}{I_c} u_m d \quad (14)$$

where α_0 is the shear stress-moment transfer coefficient at the critical section (0.4 for square column); M_{unb} is the unbalanced moment at the gravity axis of the control perimeter; c is the size

of the square column; and I_c is the property of assumed critical section analogous to the polar moment of inertia.

Eurocode 2 (2004)

Different from ACI 318-19 (2019), the Eurocode 2 (2004) specifies the critical section at a distance $2d$ from the column face. The punching shear stress $v_{Rd,c}$ of the slab-column connections under concentric loading cases can be calculated by the following expression:

$$v_{Rd,c} = 0.18k(100\rho f'_c)^{1/3} \geq v_{\min} = 0.035k^{3/2}\sqrt{f'_c} \quad (15)$$

where k is the coefficient considering size effect ($k = 1 + \sqrt{200/d} \leq 2.0$); ρ is the average flexural reinforcement ratio ($\rho = \sqrt{\rho_x \rho_y} \leq 0.02$); d is the effective depth; and f'_c is the concrete compressive strength.

For eccentric loading cases, the maximum shear stress v_{Ed} should be taken as:

$$v_{Ed} = \frac{V_{Ed}}{u_1 d} \left(1 + \frac{3}{5} \frac{M_{Ed}}{V_{Ed}} \cdot \frac{u_1}{W_1} \right) \leq v_{Rd,c} \quad (16)$$

where V_{Ed} is the applied shear force; u_1 is the critical shear perimeter; M_{Ed} is the applied internal bending moment; and W_1 is calculated for the basic control perimeter u_1 . For an internal square column, W_1 is taken as:

$$W_1 = \frac{c^2}{2} + c^2 + 4cd + 16d^2 + 2\pi dc \quad (17)$$

where c is the size of the square column.

BS 8110 (1997)

For the BS8110 (1997), the critical section at a distance $1.5d$ from the column face is assumed.

For concentric load, the punching shear strength V_c can be calculated as follow:

$$V_c = 0.79(100\rho)^{1/3} \left(\frac{400}{d} \right)^{1/4} \left(\frac{f'_c / 0.78}{25} \right)^{1/3} b_0 d \quad (18)$$

where ρ is the reinforcement ratio; b_0 is the control perimeter; d is the effective depth; and f_c' is the concrete compressive strength.

For eccentric loading, the punching shear strength V_{eff} is taken as follow:

$$V_{eff} = V_t \left(1 + \frac{1.5M_t}{V_t x} \right) \quad (19)$$

where V_t is the design shear force; x is the length of the perimeter side parallel to the axis of bending; and M_t is the design moment transmitted from the slab to the column.

Model Code 2010 (2012)

The critical section of the Model Code 2010 (2012) is defined as at a distance $d_v/2$ from the column face. The punching shear resistance $V_{Rd,c}$ can be calculated as:

$$V_{Rd,c} = k_\psi \sqrt{f_{ck}} b_0 d_v \quad (20)$$

$$k_\psi = \frac{1}{1.5 + 0.9 k_{dg} \psi d} \leq 0.6 \quad (21)$$

where f_{ck} is the characteristic value of compressive strength of concrete; b_0 is the control perimeter; d_v is the shear-resisting effective depth of the slab; k_{dg} is the aggregate size influence parameter, $k_{dg} = 32 / (16 + d_g) \geq 0.75$ for the maximum aggregate size $d_g < 16$ mm and $k_{dg} = 1.0$ for $d_g \geq 16$ mm; d is the effective depth of the slab; For Level II of approximation, the slab rotation ψ can be calculated as:

$$\psi = 1.5 \cdot \frac{r_s}{d} \cdot \frac{f_{yd}}{E_s} \cdot \left(\frac{m_{Ed}}{m_{Rd}} \right)^{1.5} \quad (22)$$

where r_s is the position where the radial bending moment is zero with respect to the support axis; E_s is the modulus of elasticity of reinforcing steel; f_{yd} is the yield strength of reinforcing steel; m_{Ed} is the average moment per unit length for calculation of the flexural reinforcement in the support strip; m_{Rd} is the average flexural strength per unit length in the support strip.

For inner columns, m_{Ed} can be calculated as:

$$m_{Ed} = V_{Ed} \left(\frac{1}{8} + \frac{|e_{u,i}|}{2 \cdot b_s} \right) \quad (23)$$

where $e_{u,i}$ is the eccentricity of the resultant of shear forces with respect to the centroid of the basic control perimeter; V_{Ed} is the shear force with respect to punching; b_s is the width of the support strip, $b_s = 1.5 \cdot \sqrt{r_{s,x} \cdot r_{s,y}}$; m_{Rd} can be calculated as:

$$m_{Rd} = \rho \cdot f_{yd} \cdot d^2 \cdot \left(1 - \frac{\rho \cdot f_{yd}}{2 \cdot f_{ck}} \right) \quad (24)$$

where ρ is the reinforcement ratio.

The effect of eccentric loading can approximately be included by multiplying the length of the reduced basic control perimeter $b_{1,red}$ by the coefficient of eccentricity k_e :

$$b_0 = k_e \cdot b_{1,red} \quad (25)$$

$$k_e = \frac{1}{1 + e_u / b_u} \quad (26)$$

where e_u is the eccentricity of the resultant of shear forces with respect to the centroid of the basic control perimeter; and b_u is the diameter of a circle with the same surface as the region inside the basic control perimeter.

It should be noted that the parameters used in the above formulae are the experimental ones. Table 4 summarizes the predicted punching shear strength of the tested specimens according to these design codes. It should be noted that the results of Eurocode 2 (2004), BS 8110 (1997), and Model Code 2010 (2012) for the corroded specimens had already taken into account the reduction in reinforcement ratio caused by corrosion. As the reinforcement ratio is not considered in GB 50010 (2010) and ACI 318-19 (2019) explicitly, the influence of reinforcement corrosion on punching shear strength of slab-column connection is not considered in both codes. Therefore, the predicted value would be unchangeable after rebar corrosion, although the test value decreased with the increase of the corroded degree, which would result in an unconservative predicted value

($V_{test}/V_{th} < 1.0$) for the specimens with high corroded degree. These unsafe predictions may be caused by the change of failure mechanism. For Eurocode 2 (2004) and BS 8110 (1997), the result of V_{test}/V_{th} is far less than 1.0 for the specimens with relatively high corroded degree, such as Specimens C-0.52-20, E2-0.91-20, and E2-0.52-20, indicating that the formulae proposed by Eurocode 2 (2004) and BS 8110 (1997) could not predict the punching shear strength of the corroded slab-column connections well, although both codes had considered the reduction of reinforcement ratio caused by rebar corrosion. This is because the reinforcement corrosion not only reduces the reinforcement ratio, but also weakens interlocking action of the aggregate and dowel action of the rebar, which are ignored in BS 8110 (1997) and Eurocode 2 (2004). Model Code 2010 (2012) has a relatively high conservative estimation for all the uncorroded specimens. Although the value V_{test}/V_{th} of Model Code 2010 (2012) decreases with increasing the corroded degree, it is still able to maintain a conservative estimation for a relatively high corroded degree.

In summary, all these formulae in codes could not accurately predict the punching shear strength of corroded slab-column connections. Therefore, it is necessary to further study the mechanism of punching shear resistance of corroded slab-column connection. According to the critical shear crack theory (CSCT) from Muttoni (2008), the punching shear failure is caused by the opening of a critical shear crack. Based on the above assumption, Muttoni (2008) proposed a failure criterion for punching shear. This failure criterion can predict the punching shear strength of the uncorroded RC slab without transverse reinforcement accurately. After rebar corrosion, the opening of the critical shear crack would be larger than that of the uncorroded case under the same load. Therefore, a magnification factor of the crack width could be introduced in the failure criterion to consider the influence of rebar corrosion. However, as the number of tests was limited, the data measured was not enough to establish the relationship between corroded degree and

punching shear strength. Thus, it is suggested to conduct more tests to fill this gap.

Conclusions

The punching shear resistance of corroded slab-column connections under eccentric load was investigated in this study. The following conclusions were drawn based on the experimental and analytical results:

1. Comparing to the slab-column connections subjected to concentric load, the slab-column connections subjected to eccentric load show more damage, greater reinforcement strain, wider crack width, and larger deflection at the side of eccentric load due to extra stress that developed from the unbalanced moment transfer. Moreover, the existence of unbalanced moment has a great influence on the punching shear resistance of the slab-column connections. When increasing the loading eccentricity from zero to one time the column dimension, the punching shear strength decreases by 32% and 20% for the slab-column connections with reinforcement ratios of 0.91% and 0.52%, respectively.
2. The strain gauge results together with the yield-line results demonstrated that the rebar corrosion may change the failure mode of slab-column connections. C-0.52-0 and C-0.52-10 failed in flexure first, while C-0.52-20 failed in pure punching shear failure. In addition, E2-0.91-0 and E2-0.91-10 failed in pure punching shear failure, while E2-0.91-20 failed in flexure first.
3. With increasing the corroded degree, the crack widths of the slab-column connections decrease under the same load level due to the detrimental of the cracked stiffness caused by rebar corrosion. In addition, the critical failure zone of the corroded slab-column connections is larger than that of uncorroded connections, because the critical shear cracks may extend along the existing horizontal cracks, which were along the corroded reinforcement.

4. Rebar corrosion reduces the punching shear resistance of the slab-column connection. With increasing the corroded degree to about 20%, the punching shear strength of C1-0.91-20, C-0.52-20, E1-0.91-20, E2-0.92-20, and E2-0.52-20 decreased by 24.5%, 25.9%, 21.7%, 23.2%, and 24.0%, respectively, comparing to their controlled specimens. This reduction can be attributed to weakened interlocking of aggregate, dowel action of rebar, and bond strength between concrete and reinforcement caused by rebar corrosion. In addition, the slab-column connection with lower reinforcement ratio or larger loading eccentricity is more susceptible to the rebar corrosion effects.
5. Rebar corrosion may change the deformation capacity of the slab-column connections. The deformation capacity of the slab-column connections with high reinforcement ratio and small loading eccentricity may increase with increasing the corroded degree owing to lowered effective reinforcement ratio due to rebar corrosion, and consequently may lead to an increase in the energy-dissipating capacity. However, for the slab-column connections with a low reinforcement ratio and high loading eccentricity, the deformation capacity and energy-dissipating capacity decrease with increasing the corroded degree.

Data Availability

Some or all data, models, or code that support the findings of this study are available from the corresponding author upon reasonable request.

Acknowledgements

This research was supported by a research grant provided by the National Natural Science Foundation of China (Nos. 52022024, 52168028). Natural Science Foundation of Guangxi (No.2021GXNSFFA196001). Any opinions, findings and conclusions expressed in this paper are those of the writers and do not necessarily reflect the view of National Natural Science Foundation

460 of China.

461 REFERENCES

- 462 American Concrete Institute (ACI). 2019. Building code requirements for structural concrete
463 (ACI 318-19) and commentary. ACI Committee 318. Farmington Hills, MI: ACI.
- 464 Almusallam, A. A., Al-Gahtani, A. S., Aziz, A. R., *et al.* (1996). “Effect of reinforcement
465 corrosion on flexural behaviour of concrete slabs.” *Journal of Materials in Civil Engineering*,
466 8(3): 123-127.
- 467 Al-Swaidani, A. M., and Aliyan, S. D. (2015). “Effect of adding scoria as cement replacement on
468 durability-related properties.” *International Journal of Concrete Structures and Materials*,
469 9(2): 241-254.
- 470 Bazant, Z. P., and Cao, Z. P. (1987). “Size effect in punching shear failure of slabs.” *ACI Structural*
471 *Journal*, 84(6): 44-53.
- 472 BS 8110. (1997). “Structural use of concrete. Part I: Code of practice for design and construction.”
473 Br. Stand. Institution, UK.
- 474 Cairns, J., Plizzari, G. A., Du, Y., Law, D. W., and Franzoni, C. (2005). “Mechanical properties of
475 corrosion-damaged reinforcement.” *ACI Structural Journal*, 102(4): 256-264.
- 476 Castel, A., Francois, R., and Arliguie, G. (2000a). “Mechanical behaviour of corroded reinforced
477 concrete beams-part 1: experimental study of corroded beams.” *Materials and structures*,
478 33(9): 539-544.
- 479 Castel, A., Francois, R., and Arliguie, G. (2000b). “Mechanical behaviour of corroded reinforced
480 concrete beams-Part 2: Bond and notch effects.” *Materials and structures*, 33(9): 545-551.
- 481 CSA (Canadian Standards Association). (2014). “Design of concrete structures.” *CAN/CSA A23.3-*
482 *14*, Mississauga, ON, Canada.

483 Drakatos, I. S., Muttoni, A., and Beyer, K. (2018). "Mechanical model for drift-induced punching
484 of slab-column connections without transverse reinforcement." *ACI Structural Journal*, 115(2):
485 463-474.

486 Durrani, A. J., Du, Y., and Luo, Y. H. (1995). "Seismic resistance of nonductile slab-column
487 connections in existing flat-slab buildings." *ACI Structural Journal*, 92(4): 479-487.

488 European Committee for Standardization (CEN). (2004). "Design of concrete structures—Part 1-
489 1: General rules and rules for buildings." Eurocode 2, Brussels, Belgium.

490 Fédération International du Béton (fib). (2012). Model Code 2010 final completed draft, Bulletins
491 d'Informations 65 and 66. Fédération International du Béton (fib), Lusanne, Switzerland.

492 GB 50010. (2010). "Code for Design of Concrete Structures". Ministry of House and Urban-Rural
493 Development of People's Republic of China, China.

494 González, J. A., Andrade, C., Alonso, C., and Feliu, S. (1995). "Comparison of rates of general
495 corrosion and maximum pitting penetration on concrete embedded steel reinforcement."
496 *Cement and Concrete Research*, 25(2): 257-264.

497 Hawkins, N. M., Bao, A., and Yamazaki, J. (1989). "Moment transfer from concrete slabs to
498 columns." *ACI Structural Journal*, 86(70): 705-716.

499 Ikehata, S., Ishiguro, H., Nakano, T., and Nakamura, H. (2020). "Experimental evaluation of
500 punching shear capacity of reinforced concrete slabs with horizontal crack due to compression
501 rebar corrosion." *Structural Concrete*, 21(3).

502 Jang, D. H., and Shen, J. H. (1986). "Strength of concrete slabs in punching shear." *Journal of*
503 *Structural Engineering*, 112(13): 2578-2591.

504 Lee, C., Bonacci, J. F., Thomas, M. D., Maalej, M., Khajepour, S., Hearn, N., *et al.* (2000).
505 "Accelerated corrosion and repair of reinforced concrete columns using carbon fibre

reinforced polymer sheets.” *Canadian Journal of Civil Engineering*, 27(5): 941-948.

Lee, H., Noguchi, T., and Tomosawa, F. (1998). “FEM analysis for structural performance of deteriorated RC structures due to rebar corrosion.” *In Proceedings of the second international conference on concrete under severe conditions*, Tromso, Norway, 327-336.

Liu, J. R., Tian, Y., Orton, S. L., Said, A. M. (2015). “Resistance of flat-plate buildings against progressive collapse. 1: modelling of slab-column connections.” *Journal of Structural Engineering*, 141(12).

Maaddawy, T., and Soudki, K. A. (2003). “Effectiveness of impressed current technique to simulate corrosion of steel reinforcement in concrete.” *Journal of Materials in Civil Engineering*, 15(1): 41-47.

Marano, G. C., Quaranta G., Mezzina M. (2008). “Fuzzy time-dependent reliability analysis of RC beams subject to pitting corrosion.” *Journal of Materials in Civil Engineering*, 20(9): 578-587.

Marzouk, H., Emam, M., and Hilal, M. S. (1998). “Effect of high-strength concrete slab on the behaviour of slab-column connections.” *ACI Structural Journal*, 95(3): 227-237.

Marzouk, H., Osman, M., and Helmy, S. (2000). “Behavior of high-strength lightweight aggregate concrete slabs under column load and unbalanced moment.” *ACI Structural Journal*, 97(3): 860-866.

Muttoni, A. (2008). “Punching shear strength of reinforced concrete slabs without transverse reinforcement”, *ACI Structural Journal*, 105(4): 440-450.

Okada, K., Kobayashi, K., and Miyagawa, T. (1988). “Influence of longitudinal cracking due to reinforcement corrosion on characteristics of reinforced concrete members.” *Journal of Structural Engineering*, 85(2): 134-140.

- Ou, Y., Susanto, Y. T. T., and Roh, H. (2016). "Tensile behavior of naturally and artificially corroded steel bars." *Construction and Building Materials*, 103: 93-104.
- Park, R., and Gamble, W. L. (1981). "Reinforced Concrete Slabs." Wiley.
- Qian, K., and Li, B. (2015). "Strengthening of multibay reinforced concrete flat slabs to mitigate progressive collapse." *Journal of Structural Engineering*, 141(6).
- Xue, H. Z., Gilbert, B. P., Guan, H., and Lu, X. Z. (2018). "Load transfer and collapse resistance of RC flat plates under interior column removal scenario." *Journal of Structural Engineering*, 144(7).
- Xue, H. Z., Guan, H., Gilbert, B. P., and Lu, X. Z. (2020). "Comparative and parametric studies on behavior of RC-flat plates subjected to interior-column loss" *Journal of Structural Engineering*, 146(9).
- Teng, S., Chanthabouala, K., Lim, D. T. Y., and Hidayat, R. (2018). "Punching shear strength of slabs and influence of low reinforcement ratio." *ACI Structural Journal*, 115(6):1815-1815.
- Tian, Y., Jirsa, J. O., Widiyanto, O. B., and Argudo, J. F. (2008). "Behavior of slab-column connections of existing flat-plate structures." *ACI Structural Journal*, 105(5):561-569.

FIGURE CAPTIONS

Fig. 1. Dimensions and reinforcement details

Fig. 2. Accelerated corrosion test setup

Fig. 3. Test setup

Fig. 4. Surface condition of E1-0.91-20 after the corrosion process

Fig. 5. Crack patterns and critical failure zones of specimens subjected to concentric load

Fig. 6. Crack patterns and critical failure zones of specimens subjected to eccentric load

Fig. 7. Relationship between crack width and load: (a) C-0.91 and E1-0.91 series; (b) E2-0.91 Fig.

Fig. 8. Reinforcement strain profile of uncorroded specimens at the failure load

Fig. 9. Load-displacement curves of the specimens: (a) C-0.91 and E1-0.91 series; (b) E2-0.91 series; (c) C-0.52 and E2-0.52 series

Fig. 10. Deflection profiles of the specimens at failure load: (a) C-0.91 and C-0.52 series; (b) E1-0.91 and E2-0.91 series

Fig. 11. Typical yield-line patterns: (a) C series; (b) E series

Table 1. Characteristics of Specimens

	Specimen ID	Slab dimensions (m)	Column size (mm)	e (mm)	f'_c (MPa)	Bottom reinforcement (mm)	ρ (%)	Target corroded degree (%)
C-0.91 Series	C-0.91-0				36.3			0
	C-0.91-10	2.2×2.2×0.15	200	0	39.3	T12@105	0.91	10
	C-0.91-20				41.1			20
C-0.52 Series	C-0.52-0				43.7			0
	C-0.52-10	2.2×2.2×0.15	200	0	44.1	T12@190	0.52	10
	C-0.52-20				45.6			20
E1-0.91 Series	E1-0.91-0				38.0			0
	E1-0.91-10	2.2×2.2×0.15	200	100	36.5	T12@105	0.91	10
	E1-0.91-20				36.5			20
E2-0.91 Series	E2-0.91-0				40.1			0
	E2-0.91-10	2.2×2.2×0.15	200	200	39.3	T12@105	0.91	10
	E2-0.91-20				39.3			20
E2-0.52 Series	E2-0.52-0				40.5			0
	E2-0.52-10	2.2×2.2×0.15	200	200	36.5	T12@190	0.52	10
	E2-0.52-20				39.3			20

Note: The clear cover of concrete is 20 mm; The maximum size of aggregate is 20mm; e is the loading eccentricity; f'_c is the compressive strength of concrete; ρ is average flexural reinforcement ratio.

573
574
575

Table 2. Corrosion result of the specimens

Specimen ID	Designated corroded degree (%)	Distribution of corroded degree from column center				Average corroded degree (%)
		0-100 mm	100-200 mm	200-300 mm	300-400 mm	
		(%)	(%)	(%)	(%)	
C-0.91-10	10	11.8	14.2	7.0	5.4	9.6
C-0.91-20	20	20.9	28.2	9.5	11.8	17.6
C-0.52-10	10	11.6	7.8	7.3	5.9	8.1
C-0.52-20	20	10.5	16.6	8.9	16.1	13.0
E1-0.91-10	10	7.1	7.7	6.4	4.6	6.4
E1-0.91-20	20	18.2	18.8	13.8	14.6	16.4
E2-0.91-10	10	9.6	10.3	6.6	5.6	8.0
E2-0.91-20	20	21.0	22.5	15.7	12.7	17.9
E2-0.52-10	10	6.4	7.5	7.0	4.2	6.3
E-0.52-20	20	31.0	18.8	7.4	4.5	15.4

576
577
578
579
580

Table 3. Summary of Test Results

	Specimen ID	V_u (kN)	M_u (kN·m)	$v_u/\sqrt{f'_c}$	R_{cone}	Energy dissipation (kN·mm)	P_{flex} (kN)	M_{flex} (kN·m)	V_u/P_{flex} or M_u/M_{flex}	Failure mode
C-0.91 Series	C-0.91-0	376	-	62.4	$2.6d_0$	3115	436	-	0.86	P
	C-0.91-10	335	-	53.4	$4.0d_0$	3385	386	-	0.87	P
	C-0.91-20	302	-	47.1	$3.4d_0$	5096	366	-	0.83	P
C-0.52 Series	C-0.52-0	280	-	42.4	$3.3d_0$	6669	265	-	1.06	F
	C-0.52-10	244	-	36.7	$4.2d_0$	4504	241	-	1.01	F
	C-0.52-20	212	-	31.4	$3.7d_0$	3889	230	-	0.92	P
E1-0.91 Series	E1-0.91-0	324	32.4	52.6	$3.2d_0$	2327	-	64.4	0.50	P
	E1-0.91-10	294	29.4	48.7	$3.3d_0$	2370	-	53.6	0.55	P
	E1-0.91-20	249	24.9	41.2	$4.9d_0$	2713	-	42.0	0.59	P
E2-0.91 Series	E2-0.91-0	267	53.4	42.2	$3.6d_0$	1457	-	70.7	0.75	P
	E2-0.91-10	241	48.2	38.4	$4.7d_0$	1250	-	56.3	0.85	P
	E2-0.91-20	203	40.6	32.4	$3.7d_0$	937	-	40.7	1.00	F
E2-0.52 Series	E2-0.52-0	215	43.0	33.8	$2.7d_0$	2519	-	35.1	1.22	F
	E2-0.52-10	184	36.8	30.5	$2.8d_0$	1951	-	29.9	1.23	F
	E2-0.52-20	161	32.2	25.7	$4.0d_0$	1366	-	21.5	1.49	F

581 Note: V_u is the failure load; R_{cone} is the radius of the critical failure zone; d_0 is the slab thickness; P_{flex} and M_{flex} are the flexural
582 strength calculated by Eq. (3) and Eq.(9), respectively; P and F represent the failure mode of punching shear failure and flexural-
583 punching failure, respectively.

584
585
586
587
588

589
590
591

Table 4. Comparison between tests results and predictions

Specimen ID	ACI 318-19 (kN)		GB 50010 (kN)		Eurocode 2 (kN)		BS 8110 (kN)		Model Code (kN)	
	V_{th}	$\frac{V_{test}}{V_{th}}$	V_{th}	$\frac{V_{test}}{V_{th}}$	V_{th}	$\frac{V_{test}}{V_{th}}$	V_{th}	$\frac{V_{test}}{V_{th}}$	V_{th}	$\frac{V_{test}}{V_{th}}$
C-0.91-0	298	1.26	284	1.33	275	1.21	334	1.13	285	1.32
C-0.91-10	310	1.08	294	1.14	308	1.09	331	1.01	275	1.22
C-0.91-20	317	0.95	305	0.99	304	0.99	326	0.92	263	1.15
C-0.52-0	327	0.86	315	0.89	275	1.02	295	0.95	234	1.20
C-0.52-10	329	0.74	315	0.77	268	0.91	288	0.85	221	1.10
C-0.52-20	334	0.63	326	0.65	265	0.80	285	0.74	215	0.99
E1-0.91-0	224	1.45	212	1.53	285	1.14	293	1.11	228	1.42
E1-0.91-10	219	1.34	207	1.42	275	1.07	282	1.04	217	1.35
E1-0.91-20	219	1.14	207	1.20	268	0.93	272	0.92	203	1.23
E2-0.91-0	181	1.47	171	1.35	235	1.14	298	0.90	193	1.38
E2-0.91-10	180	1.34	169	1.24	227	1.06	288	0.84	182	1.32
E2-0.91-20	173	1.17	169	1.04	218	0.93	277	0.73	170	1.19
E2-0.52-0	182	1.18	174	1.23	195	1.10	246	0.87	151	1.42
E2-0.52-10	173	1.06	164	1.12	185	0.99	232	0.79	140	1.31
E2-0.52-20	179	0.90	164	0.98	183	0.88	230	0.70	134	1.20
Average		1.10		1.13		1.02		0.90		1.25
SD		0.24		0.23		0.11		0.13		0.12
COV		0.21		0.21		0.11		0.14		0.09

592
593

Note: V_{test} is the measured punching shear strength; V_{th} is the punching shear strength predicted by the codes; SD is the standard deviation; COV is the coefficient of variation.

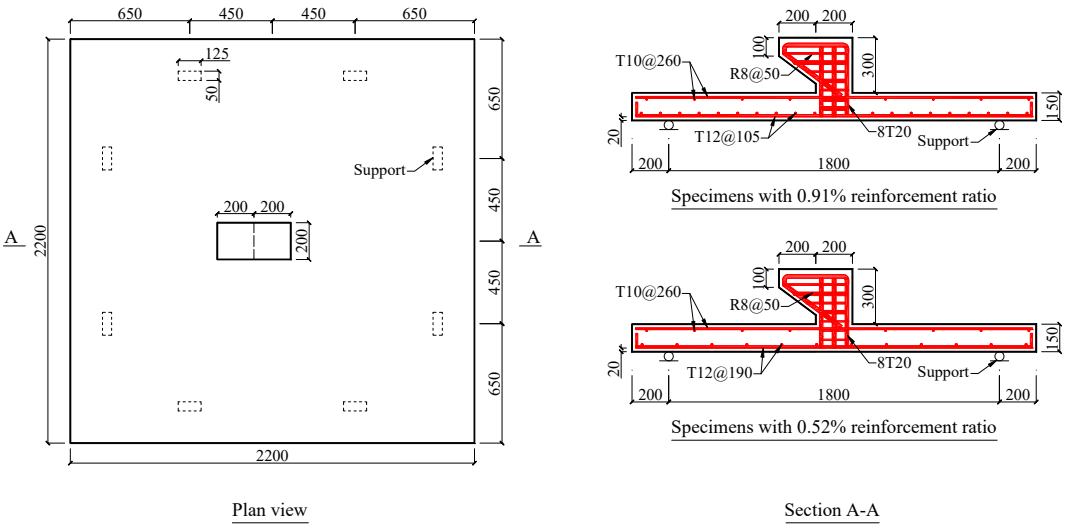
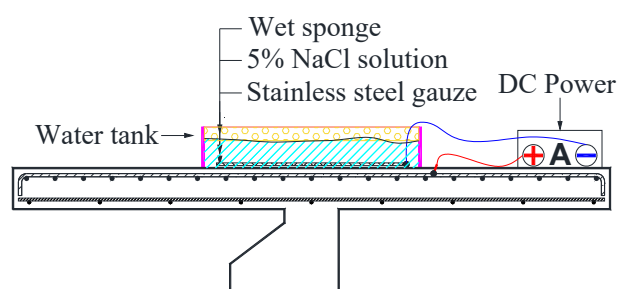
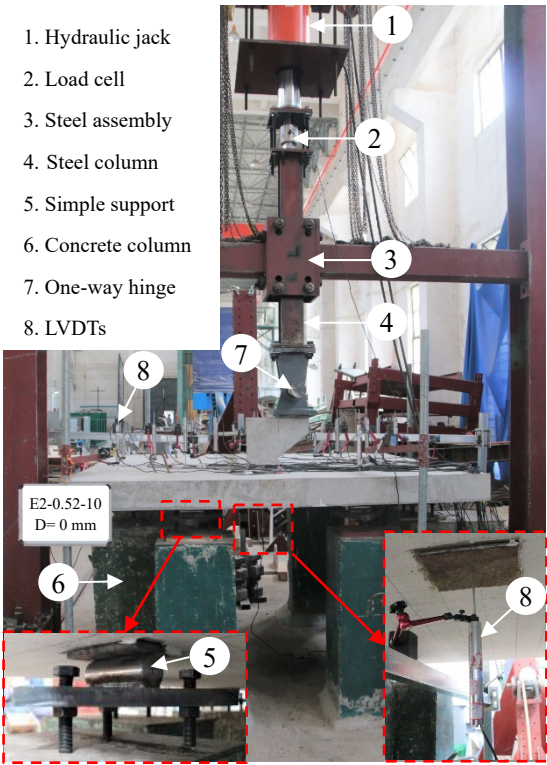
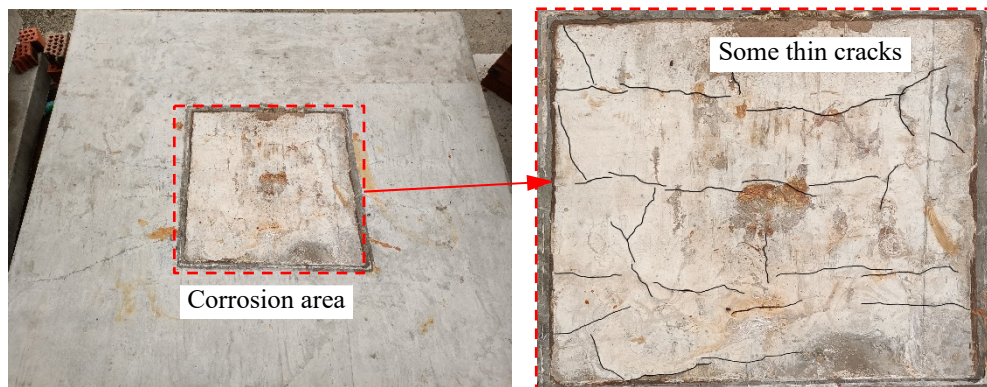
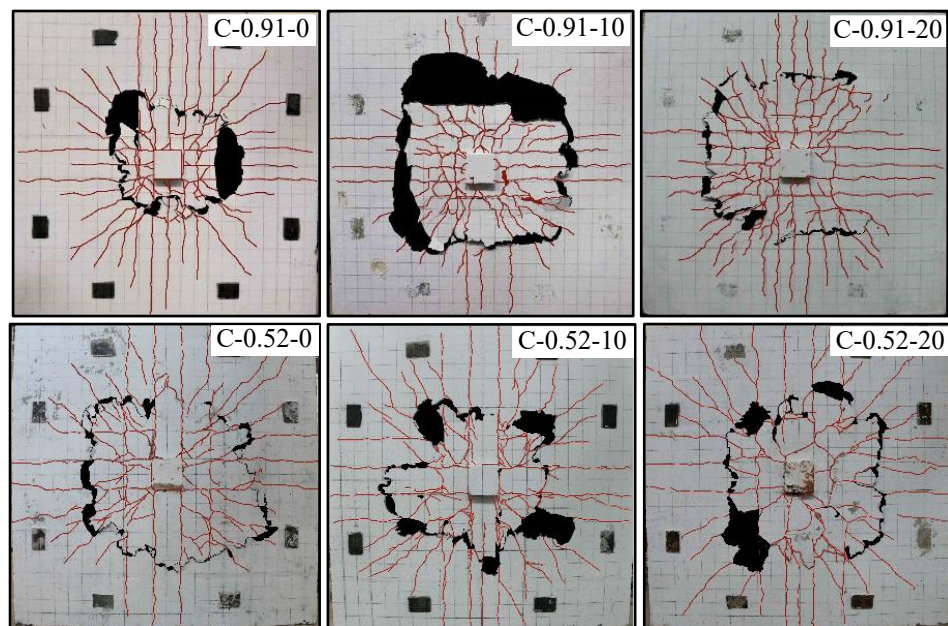


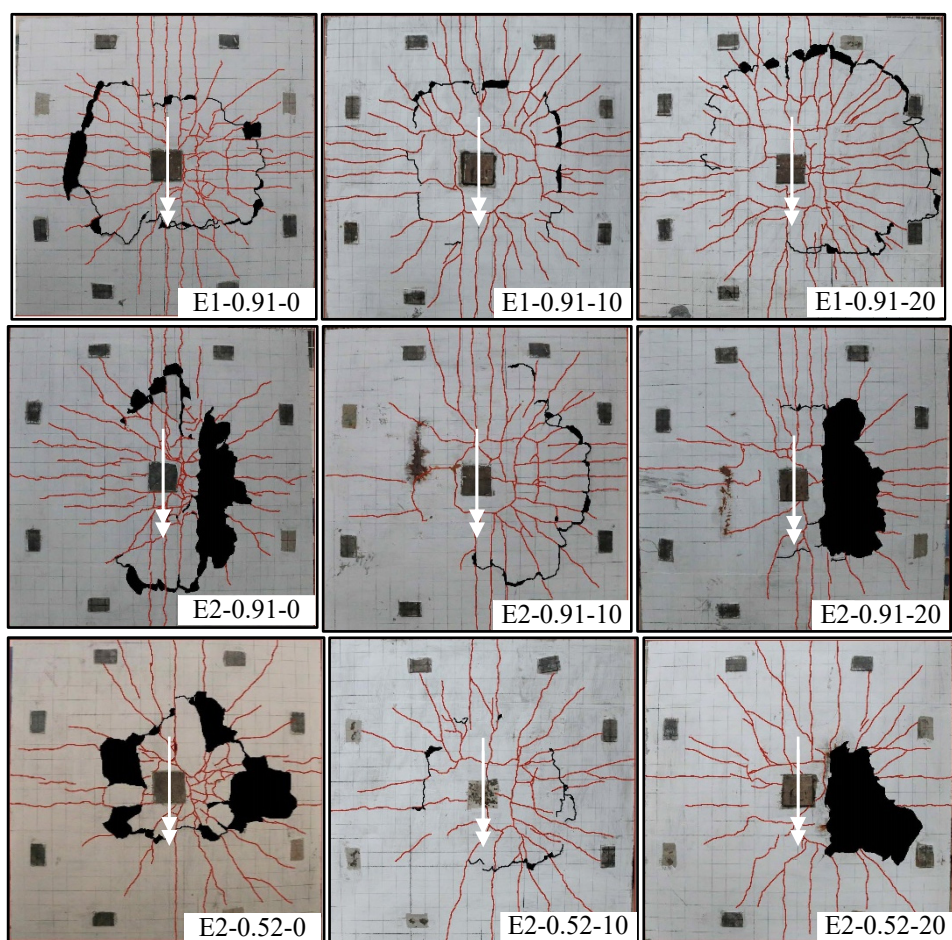
Fig. 1. Dimensions and reinforcement details

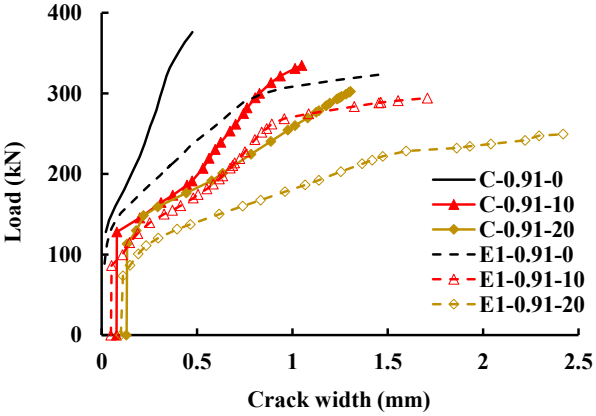




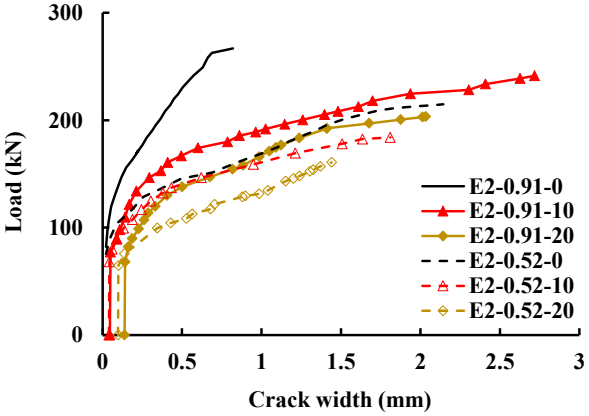




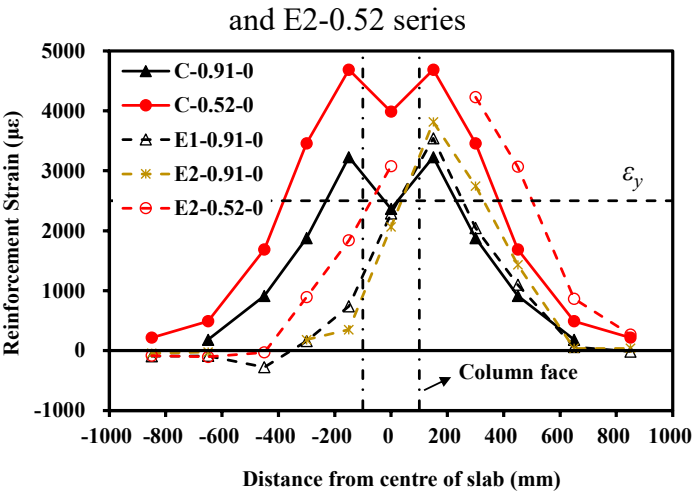


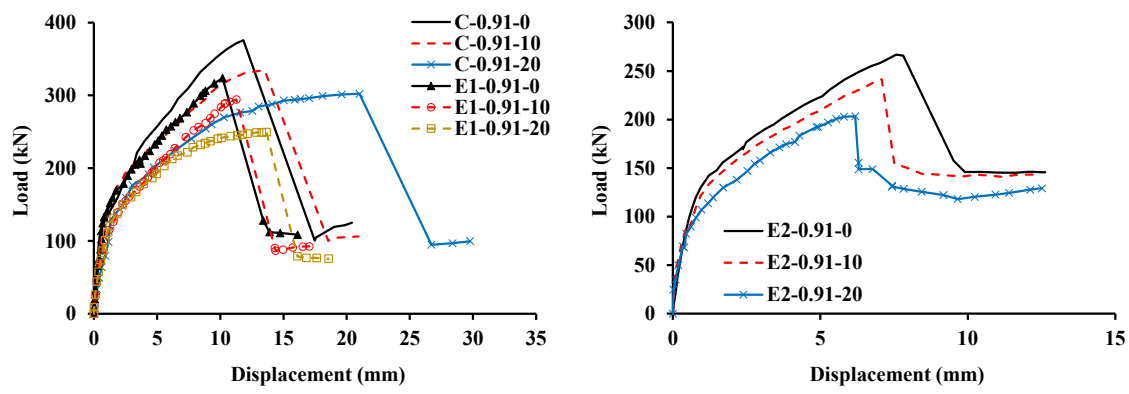


(a)



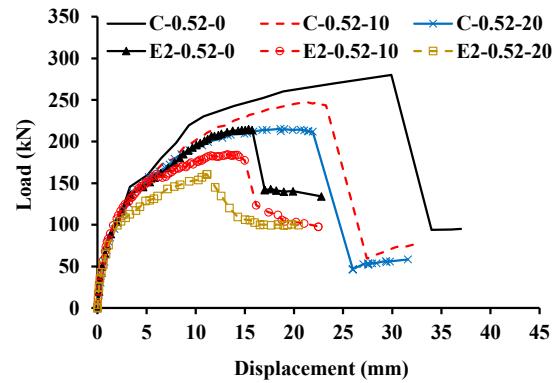
(b)



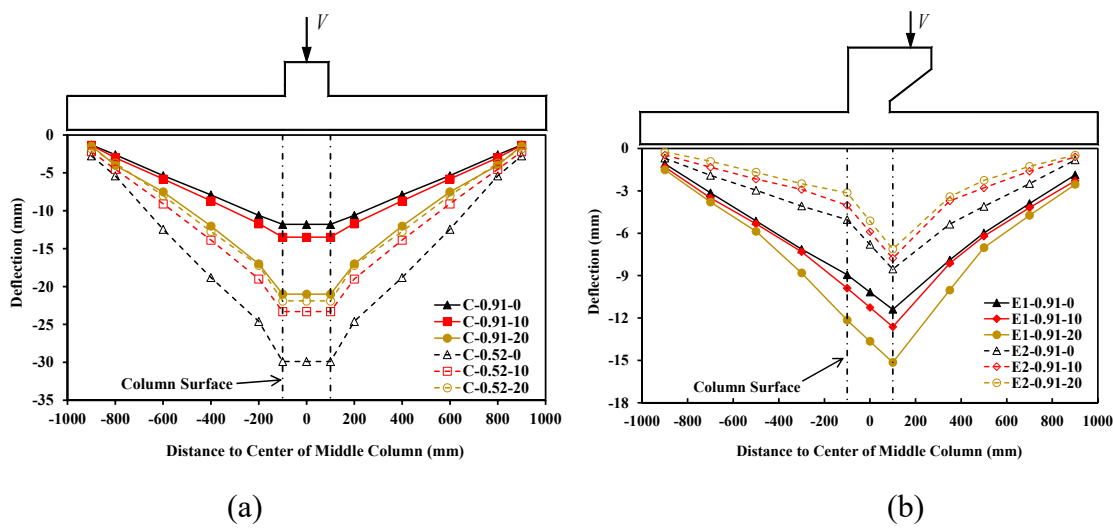


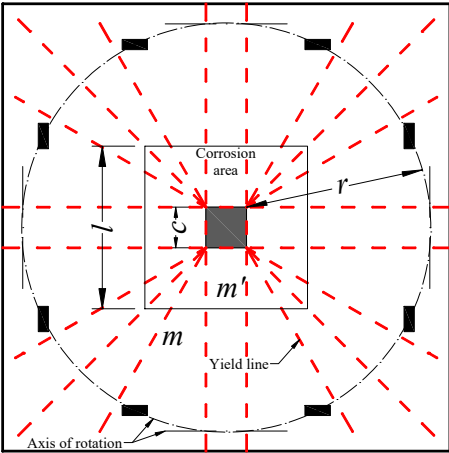
(a)

(b)

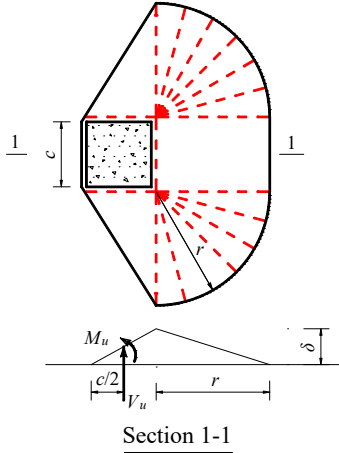


(c)





(a)



(b)